# Nucleobase Methylation Enhances SARS-CoV-2 Chain Terminator Evasion of Exonuclease Proofreading

Abstract:

Severe acute respiratory syndrome coronavirus 2 (SARS-CoV-2), causative agent of the COVID-19 pandemic, is a highly pathogenic and transmissible β-coronavirus characterized by frequent variant emergence. The rapid evolution of SARS-CoV-2 highlights its RNA-dependent RNA polymerase (RdRP), the conserved central machinery for viral replication and transcription, remains a valuable drug target. Nucleoside analogue (NuA) is a class of drugs exerting anti-viral effect by interfering SARS-CoV-2 genome synthesis through RNA chain incorporation by RdRP. Nevertheless, all coronaviruses encode a proofreading exoribonuclease in nonstructural protein nsp14 to excise misincoporated nucleotides that impedes the efficacy of NuAs. We investigated a range of chemically modified NuAs, including those with 2'-fluoro, 2'-O-methyl, and 3'-deoxy ribose substitutions as well as nucleobase modifications, to ascertain their RdRP chain termination effect and resistance to nsp14/nsp10 exonuclease proofreading. Through a combination of biochemical experiments and MD simulations, we elucidated the influence of these modifications on anti-viral efficiency. Our findings demonstrated that 3'-deoxy substitution offers superior chain termination and proofreading evasion abilities which can be further enhanced by nucleobase methylation. The study's comprehensive analysis not only furthers our understanding of SARS-CoV-2's molecular biology but also contributes to the strategic development of antiviral agents with the potential to combat the current pandemic and prepare for future coronavirus outbreaks.

Key words: SARS-CoV-2, RNA-dependent RNA polymerase, nucleotide analogue, exonuclease

## 1. Introduction

Since late 2019, the coronavirus disease 2019 (COVID-19), caused by the severe acute respiratory syndrome coronavirus 2 (SARS-CoV-2), has emerged as a global public health crisis with profound impacts on human health and the global economy. Although the rapid development and mass deployment of vaccines have been remarkably effective in curbing viral spread, the continuous evolution of the virus, particularly the emergence of variants of concern (VOCs), has led to immune evasion and frequent breakthrough infections. This stark reality underscores the urgent and critical need for the development of effective, broad-spectrum antiviral therapeutics to complement vaccination strategies.

Within the SARS-CoV-2 life cycle, the RNA-dependent RNA polymerase (RdRP), a complex composed of non-structural proteins nsp12, nsp7, and nsp8, serves as the core engine for viral genome replication and transcription. Due to its essential role in viral replication and its high degree of conservation across coronaviruses, the RdRP has become one of the most attractive targets for antiviral drug development. Nucleoside analogues (NuAs), a classic class of RdRP inhibitors, act by mimicking natural nucleoside substrates. Inside the host cell, they are phosphorylated into their active triphosphate forms (NuA-TPs) and are subsequently misincorporated into the nascent RNA chain by the RdRP. This incorporation can inhibit viral replication through various mechanisms, such as immediate or delayed chain termination, or by inducing error accumulation leading to "viral catastrophe." Several nucleoside analogue drugs, such as remdesivir and molnupiravir, have already been approved for the clinical treatment of COVID-19, demonstrating the effectiveness of this strategy.

However, a unique complexity of the coronavirus replication machinery is its possession of a 3'-to-5' exonuclease (ExoN) proofreading system, composed of the non-structural protein nsp14 and its cofactor nsp10. This proofreading machinery can recognize and excise misincorporated nucleotides, including many nucleoside analogues incorporated by the RdRP. This "self-repair" capability significantly diminishes the efficacy of many potential antiviral drugs and constitutes a major obstacle to the development of broad-spectrum, highly effective anti-coronavirus agents. Therefore, an ideal nucleoside analogue inhibitor must not only be efficiently recognized and incorporated by the RdRP but must also be able to effectively resist or "evade" excision by the nsp14/10 ExoN to achieve durable chain termination and completely block viral replication.

In this study, we aimed to identify and characterize novel nucleoside analogues capable of overcoming the SARS-CoV-2

proofreading mechanism. We first evaluated a series of chemically modified nucleoside analogues for their activity as chain terminators for the SARS-CoV-2 RdRP. Among the effective terminators, we then systematically compared their ability to resist cleavage by the nsp14/10 exonuclease after being incorporated into the 3' end of an RNA chain. Our results demonstrate that 5-Methyl-3'-dUTP is not only an effective immediate chain terminator, but the 5-methyl modification on its uracil base also confers potent resistance to proofreading, significantly outperforming its parent compound, 3'-dUTP. Furthermore, we found that 5-Methyl-3'-dUTP is more readily incorporated by the RdRP than 3'-dUTP and that RNA chains terminated with it cannot be re-extended even after potential cleavage. Together, these findings reveal the dual mechanism of action of 5-Methyl-3'-dUTP as an efficient, proofreading-resistant inhibitor of SARS-CoV-2, establishing it as a highly promising drug candidate and providing a new strategy for designing novel anti-coronavirus drugs that can overcome viral proofreading.

## 2. Materials and Methods

### *2.1 Constructs, expression, and purification of the nsp12/7/8 complex (RdRp)*

The nsp12/7/8 complex (RdRP) was expressed and purified in the insect cell-baculovirus system. Codon-optimized DNA sequence (BstEII-10 × His tag-nsp7-TEV site- nsp8-TEV site-nsp12-2 × strepII tag-RsrII) was chemically synthesized and cloned into the pKL-pBac backbone via BstEII and RsrII sites, initiated by a 5' ATG start codon, and flanked by two Tobacco Etch Virus (TEV) protease cleavage sites for post-translational processing. The baculovirus coding for the nsp complex was generated by transfecting the bacmid into Expi-Sf9 cells as P0 virus. P1 virus was amplified by infecting 50 ml fresh Sf9 cells at a density of $2 \times 10^6$/mL with 1 mL P0 virus. After 5 to 7 days, the clarified culture medium was filtered and supplemented with 0.5% BSA and stored at 4°C protected from light.

Expression of the recombinant proteins was carried out in High Five cells, cultured in ESF 921 serum-free medium (Expression Systems) at 27 °C. At a density of 2-3 million cells per mL, 200 mL of High Five cells was infected with 10 mL P1 virus for 3 to 5 days. The cells were harvested by centrifugation at 500 × g for 5 min, and the resultant cell pellets were promptly frozen and preserved at −80 °C for further analysis.

The insect cells pellets harboring the co-expressed RdRp complex were resuspended in a binding buffer composed of 50 mM HEPES (pH 7.4), 250 mM NaCl, 5 mM $MgCl_2$, 1 mM dithiothreitol (DTT), and 10% (v/v) glycerol, supplemented with an EDTA-free Protease Inhibitor Cocktail (TargetMol). Cell lysis was performed using a high-pressure homogenizer set to 500 bar. The insoluble material was removed by centrifugation at 40,000 rpm (Eppendorf himac CP100NX) for 30 min at 4 ℃, and further removed by passage through 0.45 μm filter.

Strep-Tactin®XT 4Flow® 50% suspension (IBA Lifescience) was washed with 10 volumes wash buffer and added into column. The clear supernatant from last step was added into column in flow-through mode. Then the beads were washed by 10 column volume of wash buffer (50 mM HEPES (pH 7.4), 250 mM NaCl, 5 mM $MgCl_2$, 1 mM dithiothreitol (DTT), and 10% (v/v) glycerol) and eluted with 10 column volume of elution buffer (50 mM HEPES (pH 7.4), 250 mM NaCl, 5 mM $MgCl_2$, 1 mM dithiothreitol (DTT), and 10% (v/v) glycerol, 100 mM biotin, 2 mM EDTA).

### *2.2 Constructs, expression, and purification of the nsp14/10 complex*

The nsp14/10 complex was expressed and purified in the insect cell-baculovirus system. Codon-optimized DNA sequence (BstEII-10xHis tag-nsp14- TEV site-nsp10-2xstrepII tag-RsrII) was synthesized and cloned into the pKL-pBac backbone via BstEII and RsrII sites. The expression and purification cleavage were conducted as described in *Constructs, expression, and purification of the nsp12/7/8 complex (RdRp)* with minor modifications.

The baculovirus coding for the nsp complex was generated by transfecting the bacmid into Expi-Sf9 cells as P0 virus. P1 virus was amplified by infecting 50 ml fresh Sf9 cells at a density of $2 \times 10^6$/mL with 1 mL P0 virus. After 5 to 7 days, the clarified culture

medium was filtered and supplemented with 0.5% BSA and stored at 4°C protected from light.

Expression of the recombinant proteins was carried out in High Five cells, cultured in ESF 921 serum-free medium (Expression Systems) at 27 °C. At a density of 2-3 million cells per mL, 200 mL of High Five cells was infected with 10 mL P1 virus for 3 to 5 days. The cells were harvested by centrifugation at 500 × g for 5 min, and the resultant cell pellets were promptly frozen and preserved at −80 °C for further analysis.

The insect cells pellets harboring the co-expressed nsp14/10 complex were resuspended in a binding buffer composed of 50 mM HEPES (pH 7.4), 250 mM NaCl, 5 mM $MgCl_2$, 1 mM dithiothreitol (DTT), and 10% (v/v) glycerol, supplemented with an EDTA-free Protease Inhibitor Cocktail (TargetMol). Cell lysis was performed using a high-pressure homogenizer set to 500 bar. The insoluble material was removed by centrifugation at 40,000 rpm (Eppendorf himac CP100NX) for 30 min at 4 ℃, and further removed by passage through 0.45 μm filter.

BeyoGold™ His-tag Purification Resin (Beyotime) was washed with 10 volumes wash buffer and added into column. 200 mL cell lysate was added into column in flow-through mode. Then the beads were washed by 510 column volume of wash buffer (50 mM HEPES (pH 7.4), 250 mM NaCl, 5 mM $MgCl_2$, 1 mM dithiothreitol (DTT), and 10% (v/v) glycerol) and eluted with 10 column volume of elution buffer (50 mM HEPES (pH 7.4), 250 mM NaCl, 5 mM $MgCl_2$, 1 mM dithiothreitol (DTT), and 10% (v/v) glycerol, 250 mM imidazole). The eluted buffer was further purified with Streptavidin beads as below.

Strep-Tactin®XT 4Flow® 50% suspension (IBA Lifescience) was washed with 10 volumes wash buffer and added into column. Eluted buffer from Ni-NTA resin purification was added into column in flow-through mode. Then the beads were washed by 10 column volume of wash buffer (50 mM HEPES (pH 7.4), 250 mM NaCl, 5 mM $MgCl_2$, 1 mM dithiothreitol (DTT), and 10% (v/v) glycerol) and eluted with 10 column volume of elution buffer (50 mM HEPES (pH 7.4), 250 mM NaCl, 5 mM $MgCl_2$, 1 mM dithiothreitol (DTT), and 10% (v/v) glycerol, 100 mM biotin, 2 mM EDTA).

*2.3 RdRp Enzymatic Activity Assay and Its Inhibition by Nucleotide Analogues*

In this assay, a fluorescence-labeled short RNA oligonucleotide, referred to as LS2U, with the sequence 5'-FAM-GUCAUUCUCCUAAGAAGCUU-3', was used as the primer strand. For the template strand, a longer RNA oligonucleotide named LS15A, with the sequence 5'-CUAUCCCCAUGUGAUUUUACAAGCUUCUUAGGAGAAUGAC-3', was employed. The SARS-CoV-2 RdRp (RNA-dependent RNA polymerase) complex, purified from insect cells, was utilized at a final concentration of 1 μM. The RdRp complex was incubated with 0.1 μM of the double-stranded RNA and 100 μM of rNTPs (ribonucleoside triphosphates) in a reaction buffer. This buffer was composed of 20 mM Tris (pH 7.5), 15 mM NaCl, and 5 mM $MgCl_2$. All components were prepared with RNase-free water to ensure the purity of the reaction. The total volume of the reaction mixture was maintained at 10 μL.

After a 10-minute incubation period at 37°C, a 4 μL aliquot of the reaction mixture was combined with 4 μL of 2x RNA loading buffer, which included formamide and EDTA. The combined sample (8 μL in total) was then loaded onto a 10% Urea-PAGE gel for denaturation analysis. Electrophoresis was conducted at 300V for 20 minutes, followed by imaging with a LI-COR Odyssey M Imager.

The procedure for evaluating the inhibition of the RdRp enzymatic activity by nucleotide analogues was essentially identical to the RdRp enzymatic assay described above. However, in the inhibition assays, each nucleotide analogue was introduced at a final concentration of 100 μM, replacing the corresponding NTP.

*2.4 Exonuclease Activity Assays with Nucleotide Analogue Substitution*

The 5′-fluorescein-labeled oligonucleotide, LS2U, previously mentioned in the RdRp Enzymatic Activity Assay, was prepared at a concentration of 0.1 μM. It was combined with an equimolar amount of the complementary strand, LS15A-RNA. This duplex was then introduced into a reaction buffer composed of 20 mM Tris (pH 7.5) and 5 mM MgCl2. The enzymatic reaction was initiated by the addition of 1 μM of the SARS-CoV-2 RdRp (RNA-dependent RNA polymerase) complex and a rNTP mix at a concentration of 100 μM, with each nucleotide analogue substituting for the corresponding rNTP. The mixture was incubated at 37°C for 10 minutes to form stalled RNA products. This was followed by the addition of a series of dilutions of the nsp14–nsp10 complex, with a further incubation at 37°C for an additional 10 minutes. The reactions were halted by the introduction of 2x RNA loading buffer. The resulting reaction products were resolved on a 10% TB-Urea polyacrylamide gel and were visualized using a LI-COR Odyssey M Imager.

*2.5 Exonuclease Activity Assay by Fluorescence Polarization*

The exonuclease activity of the SARS-CoV-2 nsp14/nsp10 complex and its sensitivity to nucleotide analogues were assessed in real-time using a fluorescence polarization (FP)-based assay.

The fluorophore-labeled RNA substrates, FAM-LS2U-G-3’-dU and FAM-LS2U-G-5-Methyl-3’-dU, were enzymatically synthesized by the SARS-CoV-2 RNA-dependent RNA polymerase (RdRp). Briefly, reactions contained 20 mM Tris-HCl (pH 7.5), 5 mM $MgCl_2$, 0.1 μM FAM-LS2U primer, 0.1 μM LS15A template, 2 μM nsp12/7/8 complex, 25 μM GTP, and 25 μM UTP or its respective analogue (3’-dUTP or 5-Methyl-3’-dUTP). After incubation at 37°C for 10 min, the products were purified using an RNA cleanup kit (New England Biolabs) and eluted in nuclease-free water. The concentration and integrity of the purified substrates were confirmed by denaturing PAGE.

Real-time exonuclease reactions were performed in black, round-bottom 384-well plates (Corning) in a total reaction volume of 5 μL. The standard reaction buffer consisted of 20 mM Tris-HCl (pH 7.5) and 5 mM $MgCl_2$. Each well contained 0.05 μM of the specified FAM-labeled RNA substrate. Reactions were initiated by the addition of 10 nM nsp14/nsp10 complex. The plate was immediately transferred to a pre-equilibrated BMG LABTECH CLARIOstar microplate reader maintained at 25°C.

Fluorescence polarization (measured in millipolarization units, mP) was monitored every minute for a period of 60 minutes using the following instrument settings: excitation at 482 nm (15 nm bandwidth), emission detection at 530 nm (15 nm bandwidth), and a settling time of 0.5 seconds per read. The raw mP values were exported and analyzed in GraphPad Prism (version 9.0). The initial rate of the reaction for each substrate was determined by calculating the slope of the linear phase of the mP versus time curve.

## 3. Results

*3.1 Screening of Nucleoside Analogues (NuAs) for Chain Termination Activity*

To identify potential inhibitors of the SARS-CoV-2 RNA-dependent RNA polymerase (RdRP), we investigated a panel of nucleoside analogues (NuAs) whose chemical structures are shown in Figure 1. The NuAs included 2'OMe-NTP, 2'-Fluoro-dNTP, 3'-dNTP, 5-Methyl-3'-dUTP, 6-Aza-UTP, and 3'-(O-Propargyl)-GTP. We evaluated their ability to act as chain terminators during RNA synthesis by the viral RdRP complex using RNA extension assays. The LS2U (20nt) primer labeled with FAM at the 5' end was used in all assays. For GTP and UTP analogue evaluation, the LS15 (40nt) template was paired with FAM-LS2U (Figure 2A), while the LS41-GU (41nt) template combined with FAM-LS2U was used for CTP and ATP analogue evaluation (Figure 2D).

As shown in Figure 2B, 2'OMe-GTP, 2'-Fluoro-dGTP, and 3'-dGTP were incorporated into the LS2U primer by RdRP, evidenced by the appearance of +1 bands in the absence of UTP, ATP, and CTP (Figure 2B, lanes 2, 3, and 4). In contrast, 3'-(O-Propargyl)-GTP remained at the primer position, indicating its inability to be incorporated by RdRP (Figure 2B, lane 5). Upon addition of

UTP, ATP, and CTP, 2'-Fluoro-dGTP-incorporated RNA proceeded to full-length products (Figure 2B, lane 8), similar to the natural GTP control (Figure 2B, lane 6), indicating that 2'-Fluoro-dGTP does not terminate SARS-CoV-2 RdRP-mediated synthesis. Conversely, 2'OMe-GTP and 3'-dGTP predominantly remained as +1 bands even in the presence of all three NTPs (Figure 2B, lanes 7 and 9), demonstrating that both analogues function as immediate chain terminators.

We further assessed the performance of UTP analogues with different modifications. Figure 2C shows that 2'OMe-UTP, 2'-Fluoro-dUTP, 3'-dUTP, 5-Methyl-3'-dUTP, and 6-Aza-UTP were all incorporated into the LS2U primer by RdRP, producing +2 bands in the absence of ATP and CTP (Figure 2C, left panel, lanes 4-8). Upon addition of ATP and CTP, 2'-Fluoro-dUTP and 6-Aza-UTP-incorporated RNA proceeded to full-length products (Figure 2C, right panel, lanes 13 and 16), similar to the natural UTP control (Figure 2C, right panel, lane 11), indicating these analogues do not terminate RNA synthesis. In contrast, 2'OMe-UTP, 3'-dUTP, and 5-Methyl-3'-dUTP remained as +2 bands in the presence of ATP and CTP (Figure 2C, right panel, lanes 12, 14, and 15), confirming their function as immediate chain terminators.

Consistently, as demonstrated in Figure 2E, 2'OMe-CTP, 2'-Fluoro-dCTP, and 3'-dCTP were incorporated into the LS2U primer by RdRP, producing +1 bands in the absence of ATP, GTP, and UTP (Figure 2E, lanes 3-5). Upon addition of the missing NTPs, 2'-Fluoro-dCTP-incorporated RNA proceeded to full-length products (Figure 2E, lane 8), similar to the natural CTP control (Figure 2E, lane 6), indicating non-terminating behavior. However, 2'OMe-CTP and 3'-dCTP predominantly remained as +1 bands in the presence of all three NTPs (Figure 2E, lanes 7 and 9), confirming their immediate terminating activity.

The observation for ATP analogues is also consistent. Figure 2F shows that 2'OMe-ATP, 2'-Fluoro-dATP, and 3'-dATP were incorporated into the LS2U primer by RdRP, producing +2 bands in the absence of GTP and UTP (Figure 2F, lanes 4-6). Upon addition of GTP and UTP, 2'-Fluoro-dATP-incorporated RNA proceeded to full-length products (Figure 2F, lane 9), similar to the natural GTP control (Figure 2F, lane 7), indicating non-terminating behavior. Conversely, 2'OMe-ATP and 3'-dATP remained as +2 bands in the presence of GTP and UTP (Figure 2F, lanes 8 and 10), demonstrating immediate chain termination.

Our systematic evaluation revealed distinct incorporation and termination profiles among the tested nucleoside analogues. 3'-(O-Propargyl)-GTP could not be incorporated by RdRP, while all other analogues were successfully incorporated. Among the incorporated analogues, 2'-Fluoro-dNTP and 6-Aza-UTP allowed continued RNA synthesis to full-length products, indicating they do not function as chain terminators. In contrast, 2'OMe-NTP, 3'-dNTP, and 5-Methyl-3'-dUTP consistently functioned as immediate chain terminators, effectively inhibiting SARS-CoV-2 RNA synthesis upon incorporation.

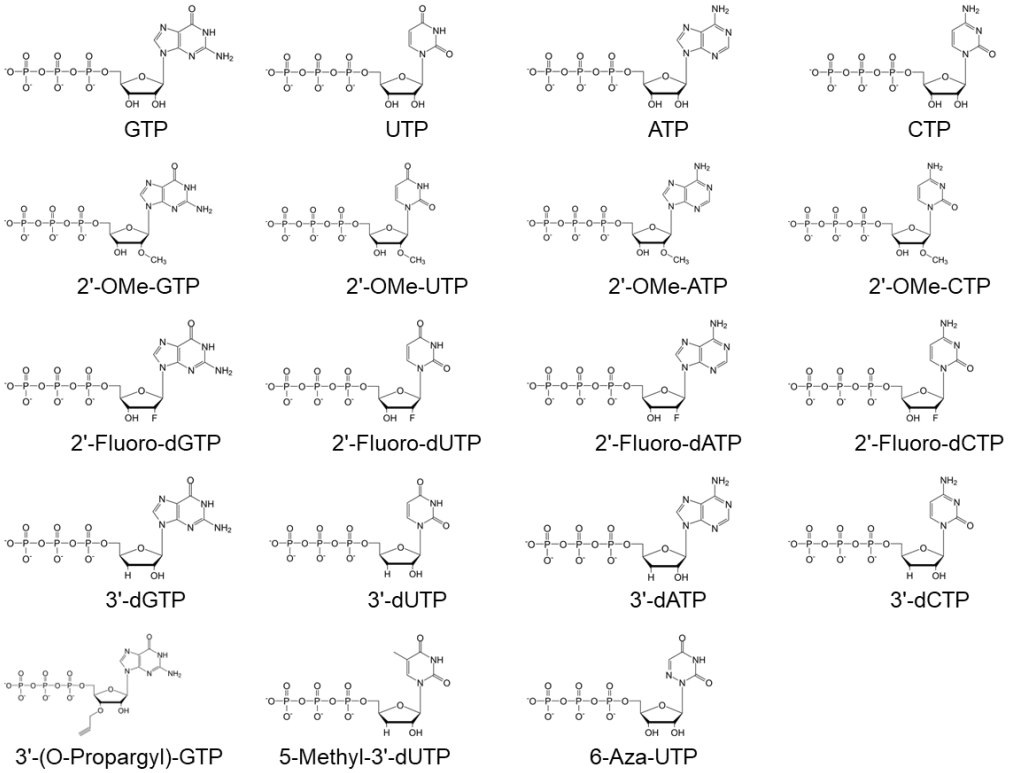


**Figure 1.** The chemical structures of the natural NTPs and NuAs employed in this study.

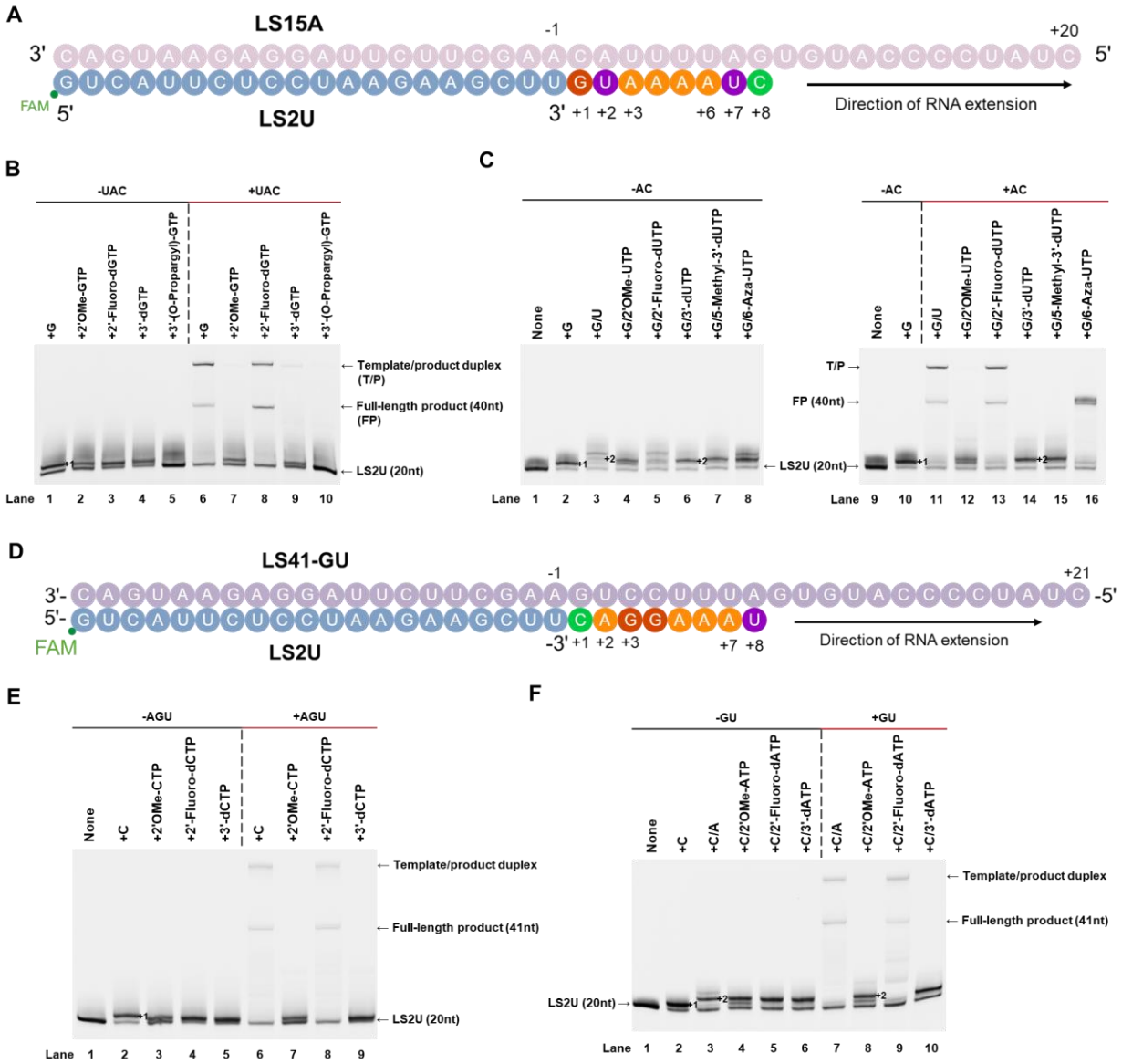


**Figure 2. Evaluation of applicability of NuA as chain terminator on SARS-CoV-2 RdRP. (A)** LS15A RNA template and LS2U RNA primer scaffolds used for RNA extension Assay (Moeller et al., 2022). The LS15A RNA template contains 40 nucleotides, and the LS2U RNA primer contains 20 nucleotides, fluorescently labelled 5′ overhang. **(B)** Incubation of the RdRp complex with LS15A-LS2U RNA duplex and each nucleotide analogue leads to efficient RNA extension, termination, or no incorporation.

*3.2 Resistance of Terminated RNA to Viral Proofreading Exonuclease (nsp14/10)*

Coronaviruses possess a proofreading exonuclease (ExoN) comprised of the nsp14/nsp10 complex, which can remove mis-incorporated nucleotides and diminish the efficacy of antiviral nucleoside analogues. To evaluate the therapeutic potential of our identified chain terminators, we assessed the stability of RNA chains terminated with 2'OMe-NTP, 3'-dNTP, and 5-Methyl-3'-dUTP against this proofreading activity using RdRP-ExoN cleavage assays (Figure 3). The experimental workflow is illustrated in Figure 3A. We used the FAM-LS2U primer paired with the LS15A template for these assays. The protocol involved a two-step process: first, the RNA template/primer duplex was incubated with SARS-CoV-2 RdRP, the corresponding NTP analogue, and the three natural NTPs at 37°C for 10 minutes to enzymatically generate analogue-terminated RNA products. Subsequently, nsp14/10 was added to the reaction and incubated for an additional 10 minutes at 37°C to assess exonucleolytic cleavage. Finally, the products were analyzed by denaturing PAGE electrophoresis.

The results revealed striking differences in exonuclease susceptibility among the tested analogues. As shown in Figure 3B, RNA

chains terminated with 2'OMe-NTP demonstrated high susceptibility to cleavage by the nsp14/10 complex. The termination effects of 2'OMe-NTP in the absence of nsp14/10 are shown in lanes 2, 4, 6, 8, and 10, while the corresponding cleavage patterns following nsp14/10 treatment are displayed in lanes 1, 3, 5, 7, and 9. The majority of 2'OMe-NMP-terminated RNA was efficiently cleaved by the proofreading exonuclease, indicating that this modification alone is insufficient to evade the viral defense mechanism. In contrast, RNA chains terminated with either 3'-dNTP or 5-Methyl-3'-dUTP exhibited remarkable resistance to exonucleolytic removal. As demonstrated in Figure 3C (lanes 1, 3, 5, 7, 9), these analogue-terminated RNAs showed only minimal cleavage by the nsp14/10 complex compared to the control conditions (lanes 2, 4, 6, 8, 10). This significant resistance to proofreading activity suggests that both 3'-dNTP and 5-Methyl-3'-dUTP possess the critical ability to evade this key viral defense mechanism, making them promising candidates for antiviral development.

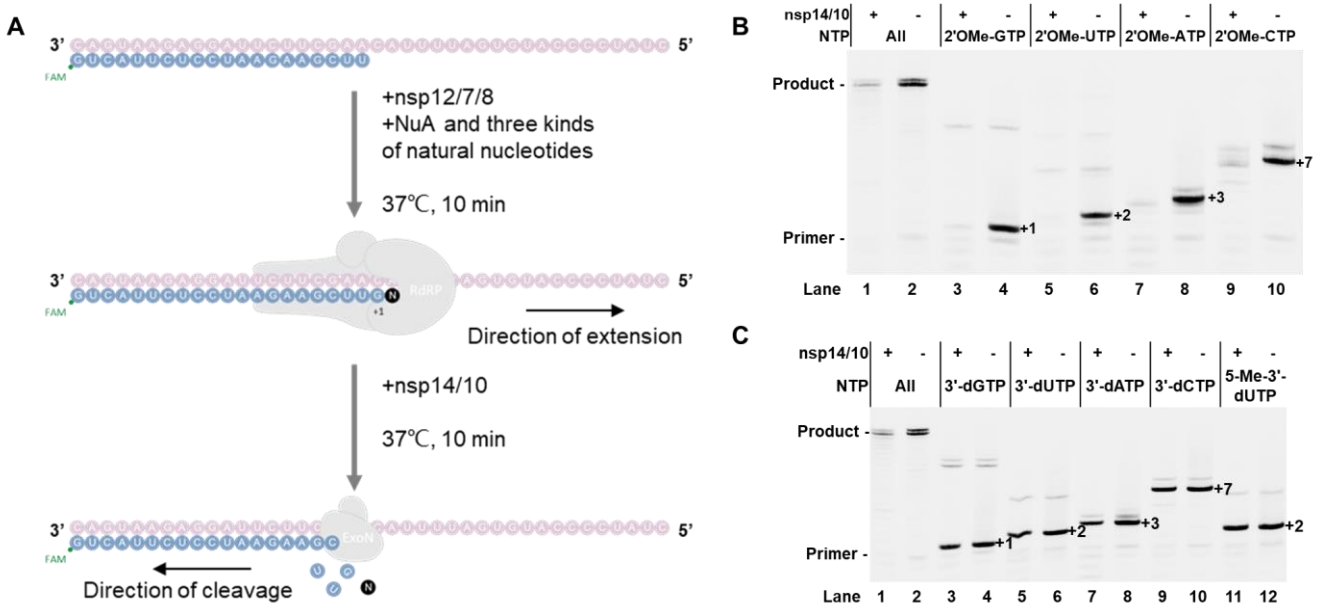


**Figure 3. RdRP-ExoN cleavage assays of 2'OMe-NTP, 3'-dNTP and 5-Methyl-3'-dUTP. (A)** Schematic of the "nucleotide analogue cleavage" experiment, result of which is shown in B and C. **(B)** Cleavage of RNA substrates incorporating 2'-O-methylated ribonucleotides by the SARS-CoV-2 nsp14/nsp10 complex. **(C)** Cleavage of RNA substrates containing 3'-deoxyribonucleotides by the SARS-CoV-2 nsp14/nsp10 complex.

*3.3 5-Methyl-3'-dUMP Confers Superior Resistance to Exonuclease Cleavage*

To determine whether the 5-methyl group on the base moiety impacts resistance against nsp14/10 proofreading mechanisms, we directly compared the cleavage susceptibility of enzymatically synthesized RNA substrates terminated with 3'-dUMP versus 5-Methyl-3'-dUMP using both concentration-dependent and time-course analyses. We employed the FAM-LS2U primer paired with the LS15A template for these comparative assays. The RNA template/primer duplex was first incubated with SARS-CoV-2 RdRP, the corresponding NTP analogue (GTP and UTP, 3'-dUTP, or 5-Methyl-3'-dUTP) at 37°C for 10 minutes to enzymatically generate UMP-, 3'-dUMP-, or 5-Methyl-3'-dUMP-terminated RNA products.

For the concentration-dependent analysis, serial dilutions of nsp14/10 were added to the respective reactions, and the products were analyzed by denaturing PAGE electrophoresis. The results demonstrated that 5-Methyl-3'-dUMP-terminated RNA exhibited significantly greater resistance to nsp14/10 cleavage compared to 3'-dUMP-terminated RNA across all tested enzyme concentrations (Figure 4A and 4C). In the time-course experiment, identical concentrations of nsp14/10 were added to each reaction and incubated for 0, 5, 10, 20, and 40 minutes before analysis by denaturing PAGE electrophoresis. Consistent with the concentration-dependent results, 5-Methyl-3'-dUMP-terminated RNA products showed markedly enhanced resistance to nsp14/10 cleavage over time compared to their 3'-dUMP counterparts (Figure 4B and 4D).

The nsp14/nsp10 exonuclease cleavage assays (Figure 4) provided clear evidence that RNA substrates containing 5-Methyl-3'-dUMP at the 3' terminus are substantially more resistant to cleavage than those ending in 3'-dUMP. This finding was further validated by real-time fluorescence polarization analysis (Figure 5A and 5B), which confirmed that 5-Methyl-3'-dUMP-terminated RNA serves as a significantly poorer substrate for the nsp14/10 exonuclease, thereby establishing the critical role of the 5-methyl modification in conferring enhanced proofreading resistance.

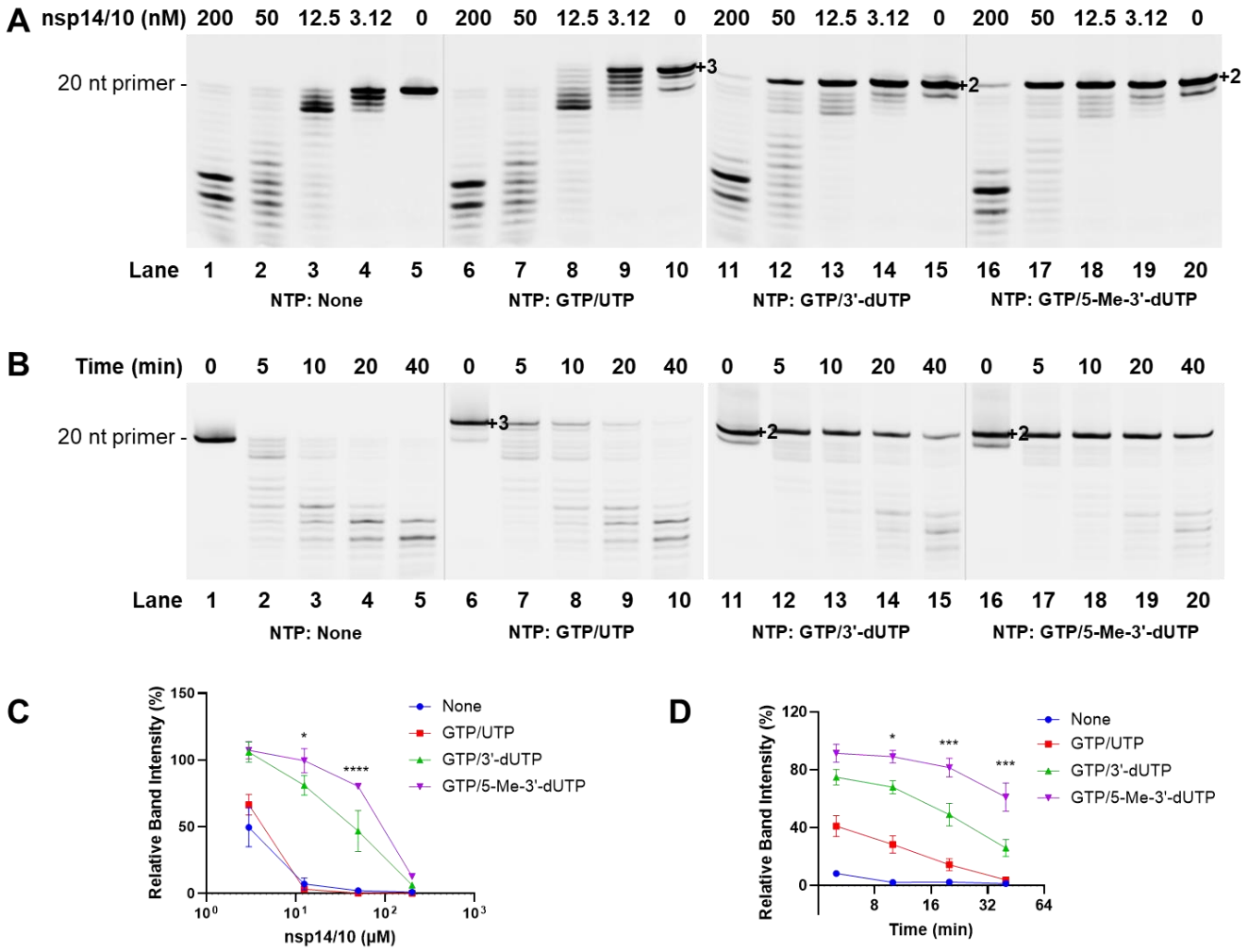


**Figure 4. Differential Cleavage of 3'-dUMP and 5-Methyl-3'-dUMP RNA Substrates by the SARS-CoV-2 nsp14/nsp10 Exonuclease. (A)** Cleavage assays of RNA substrates containing 3'-dUMP were performed with increasing concentrations of the SARS-CoV-2 nsp14/nsp10 complex. **(B)** Time-course cleavage assays of RNA substrates containing 5-Methyl-3'-dUMP by the SARS-CoV-2 nsp14/nsp10 complex. **(C)** Quantification of panel (A). Data are presented as mean ± SD from three independent experiments. **(D)** Quantification of panel (B). Data are presented as mean ± SD from three independent experiments.

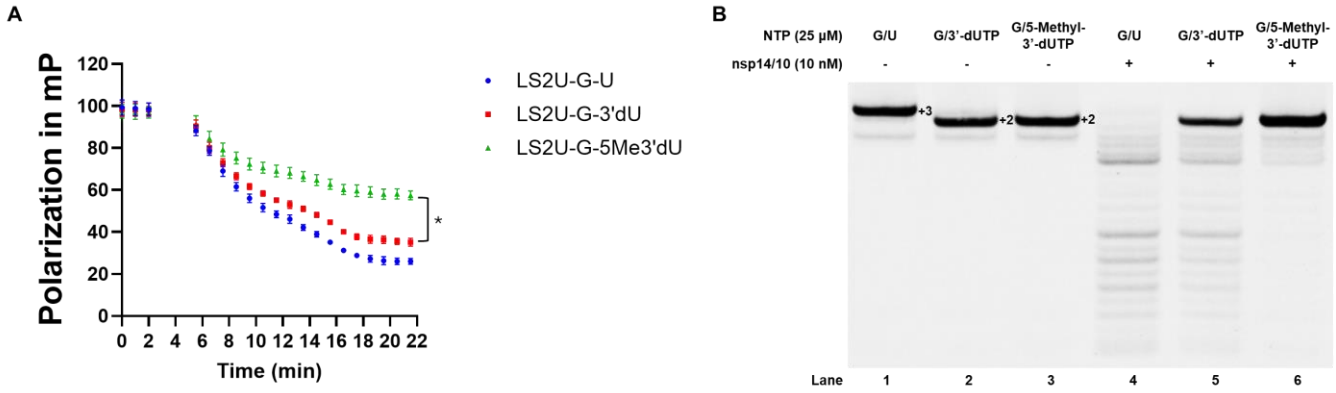


**Figure 5. Real-time analysis of nsp14/nsp10 exonuclease activity by fluorescence polarization reveals differential substrate resistance. (A)** Real-time FP signal of fluorophore-labeled RNA substrates containing 3'-dUMP or 5-Methyl-3'-dUMP upon addition of the nsp14/nsp10 complex. **(B)** Reaction products from assays corresponding to (A) were separated by denaturing PAGE.

*3.4 Incorporation Efficiency of 5-Methyl-3'-dUTP by RdRP*

An effective antiviral must be efficiently incorporated into the growing RNA chain by the viral polymerase. We therefore compared the incorporation efficiency of 5-Methyl-3'-dUTP against 3'-dUTP by the SARS-CoV-2 RdRP. The results (Figure 6) show that while natural UTP is incorporated most readily, 5-Methyl-3'-dUTP is incorporated more efficiently by RdRP than 3'-dUTP. This suggests that the 5-methyl modification improves its recognition and utilization by the viral polymerase compared to its parent compound.

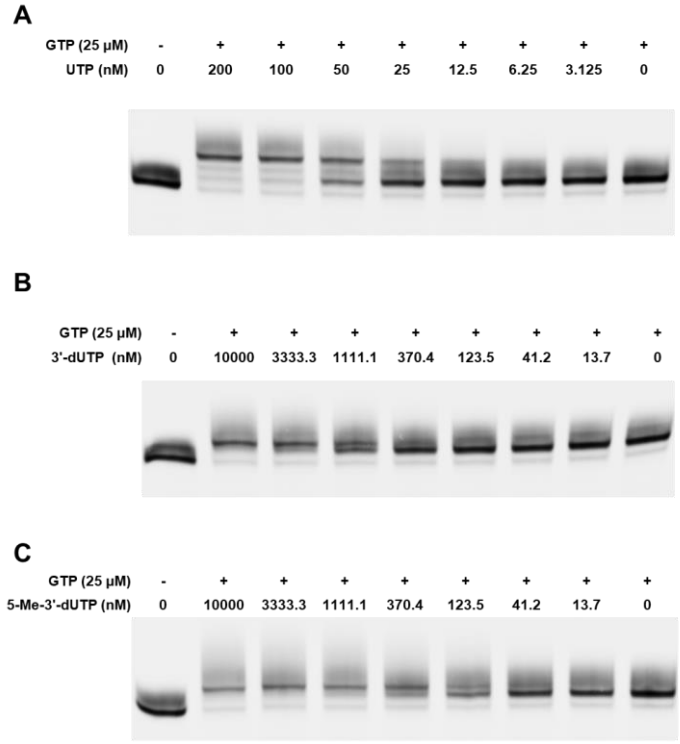


**Figure 6. Determination of $IC_{50}$ values of 3'-dUTP and 5-Methyl-3'-dUTP against SARS-CoV-2 RdRp. (A)** RNA extension reactions in the presence of increasing concentrations of 3'-dUTP. **(B)** Reactions in the presence of increasing concentrations of 5-Methyl-3'-dUTP. **(C)** Dose-response curve for 3'-dUTP, quantified from the gel in (A). **(D)** Dose-response curve for 5-Methyl-3'-dUTP., quantified from the gel in (B).

*3.5 Terminated RNA Chains Cannot Be Extended After Potential Cleavage*

Finally, we investigated the potential for RNA chain rescue if the terminal analogue were successfully removed by the nsp14/10 exonuclease. The experimental workflow is illustrated in Figure 7A. We employed the FAM-LS2U primer paired with the LS15A template for these cleavage-reextension assays. The protocol involved a multi-step process: first, the RNA template/primer duplex was incubated with SARS-CoV-2 RdRP, ATP, CTP, GTP and the corresponding NTP analogue (sofosbuvir-TP, 3'-dUTP, or 5-Methyl-3'-dUTP) at 37°C for 20 minutes to generate analogue-terminated RNA products. Subsequently, nsp14/10 and natural UTP were added to the reaction to assess whether the terminal analogue could be removed and normal synthesis resumed with the incorporation of the correct nucleotide.

As shown in Figure 7B, sofosbuvir-TP was analyzed using this method as a control based on published protocols (Moeller et al., 2022). The sofosbuvir-TP-terminated RNA was efficiently cleaved by nsp14/10 and could be subsequently extended upon addition of natural UTP, demonstrating successful rescue of the terminated RNA chain. In stark contrast, RNA chains terminated with either 3'-dUTP or 5-Methyl-3'-dUTP showed markedly different behavior. Despite treatment with nsp14/10 and supplementation with natural UTP, these analogue-terminated RNA chains could not be reextended (Figure 7C and 7D). These results indicate that 3'-dUTP and 5-Methyl-3'-dUTP effectively evade proofreading and the subsequent RdRp rescue, serving as a promising backbone for NuA design.

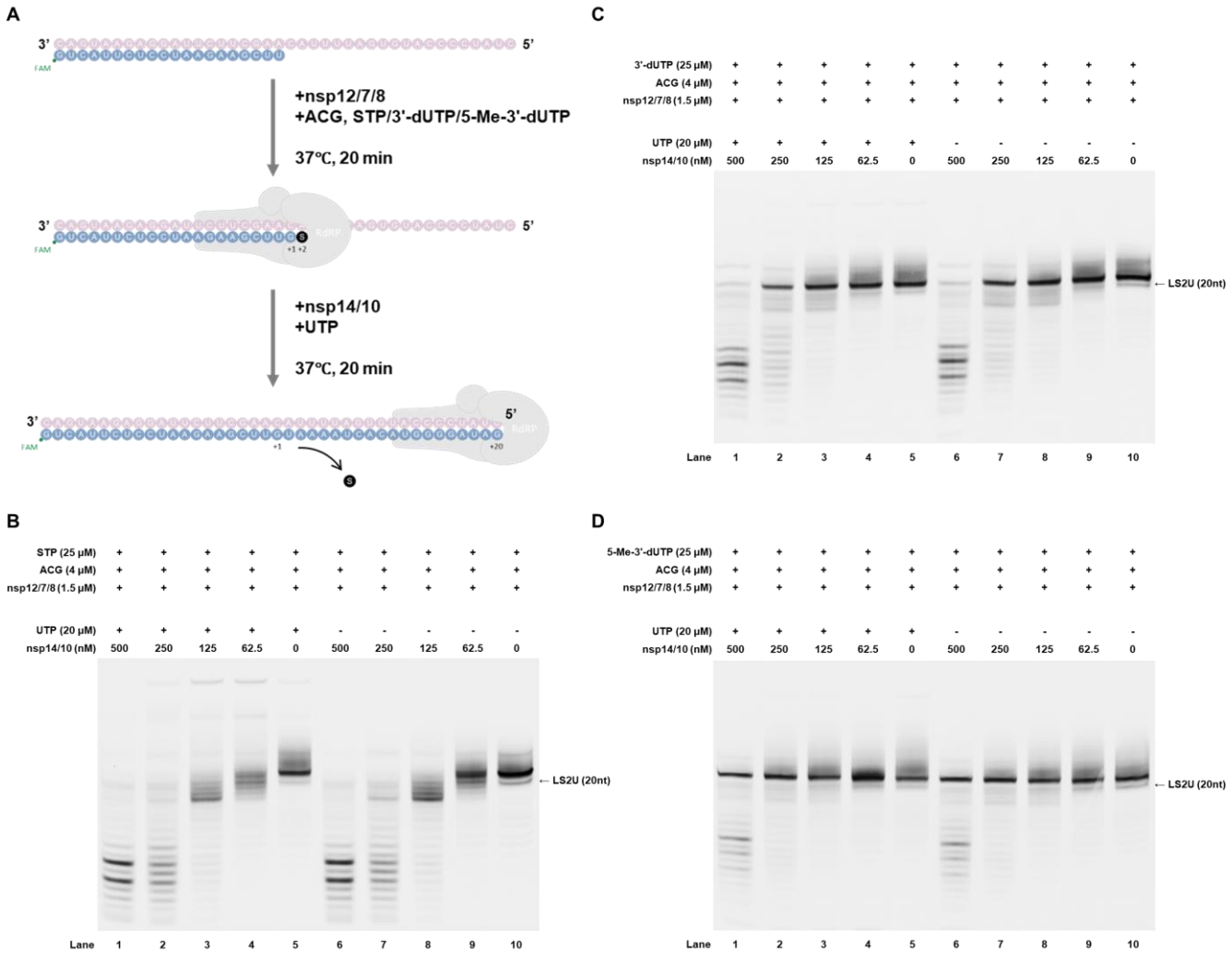


**Figure 7. Cleavage-reextension assay to evaluate RNA substrate rescue after exonuclease treatment. (A)** Experimental workflow of the cleavage-reextension assay showing the sequential steps of analogue incorporation, nsp14/10 cleavage, and subsequent RdRP-mediated reextension. **(B)** Cleavage-reextension assay results for sofosbuvir-TP-terminated RNA. **(C)** Cleavage-reextension assay results for 3'-dUTP-terminated RNA. **(D)** Cleavage-reextension assay results for 5-Methyl-3'-dUTP-terminated

RNA.

## 4. Discussion

The development of effective antiviral therapies against SARS-CoV-2 remains a critical global health priority. Nucleoside analogues that target the viral RNA-dependent RNA polymerase (RdRP) are a cornerstone of this strategy, but their efficacy can be severely compromised by the virus's proofreading exonuclease (nsp14/10), which can excise the incorporated analogue and rescue RNA synthesis. In this study, we identify and characterize 5-Methyl-3'-dUTP as a potent chain-terminating nucleoside analogue that exhibits a highly desirable dual mechanism of action: efficient incorporation by the RdRP and robust resistance to removal by the nsp14/10 proofreading machinery.

Our initial screening confirmed that 2'OMe-NTP, 3'-dNTP, and 5-Methyl-3'-dUTP act as immediate chain terminators, preventing the formation of a subsequent phosphodiester bond. However, the key differentiator for a durable antiviral lies in its ability to evade proofreading. Our results clearly showed that while RNA terminated with 2'OMe-NTP was readily cleaved by nsp14/10, both 3'-dNTP and 5-Methyl-3'-dUTP conferred significant resistance. These findings are consistent with other studies that investigated nsp14/10 cleavage of RNA substrates terminated with either 2'OMe-CMP or 3'-dCMP, which also demonstrated that 3'-dCMP-terminated RNA was more resistant to cleavage than 2'OMe-CMP-terminated RNA, which showed no resistance (Liu et al., 2021). This finding is important as it establishes that modifications at the 3' position of the ribose can, by themselves, interfere with exonuclease activity, a crucial first step in designing a proofreading-resistant inhibitor.

The central finding of our work is the superior resistance conferred by the 5-methyl modification on the uracil base. The direct comparison between 3'-dUMP and 5-Methyl-3'-dUMP terminated RNAs revealed that the latter is a significantly poorer substrate for the nsp14/10 exonuclease. We hypothesize that the methyl group at the 5-position of the base introduces steric hindrance within the active site of the nsp14 exonuclease. This steric clash likely prevents the proper positioning of the 3'-terminal nucleotide for cleavage, thereby inhibiting the proofreading function. This finding elevates the compound from an already resistant analogue (3'-dUTP) to a highly resistant one, demonstrating that a small modification on the nucleobase can be a powerful strategy to overcome viral proofreading.

Furthermore, for an analogue to be therapeutically viable, it must compete effectively with its natural counterpart for incorporation. Our data show that 5-Methyl-3'-dUTP is incorporated more efficiently by the RdRP than its parent compound, 3'-dUTP. This suggests that the 5-methyl group, far from being a hindrance, may actually enhance binding within the RdRP active site or improve its recognition as a substrate. While its incorporation is not as efficient as the natural UTP, its improved kinetics over the parent compound, combined with its profound resistance to proofreading, establishes a strong advantage for its potential as a therapeutic agent.

Our study also reveals the significance of proofreading resistant NuA scaffold. In contrast to RNA terminated with Sofosbuvir-monophosphate, which could be reextended after cleavage, we found that RNA chains terminated with either 3'-dUTP or 5-Methyl-3'-dUTP could not be rescued under the same condition. This strengthens that the "irreversible" termination is critical to render the inhibition more robust and durable.

The properties of 5-Methyl-3'-dUTP compare favorably with existing approved nucleoside analogues. Unlike remdesivir, which is a delayed chain terminator and is known to be partially susceptible to proofreading, 5-Methyl-3'-dUTP is an immediate terminator with high resistance to excision. Its mechanism is also distinct from that of molnupiravir, which functions by inducing mutagenesis rather than direct chain termination. The strategy of combining a 3'-deoxy scaffold with a 5-methyl modification on the base represents a novel and effective approach to rationally design potent and proofreading-resistant coronavirus inhibitors.

This study has several limitations. Primarily, our experiments were conducted in a purified *in vitro* setting, so key parameters such as intracellular phosphorylation efficiency, metabolic stability, cytotoxicity, and the ultimate antiviral efficacy of 5-Methyl-3'-dUTP remain undetermined. The next critical step is to design a cell-permeable prodrug of 5-Methyl-3'-dUTP, as the active triphosphate form used here cannot enter cells. While challenging, a successful prodrug would enable evaluation of antiviral activity and cytotoxicity in SARS-CoV-2 infected cell cultures. Furthermore, the potential for the virus to develop resistance via mutations in the highly conserved RdRP or nsp14 was not investigated and may require long-term clinical evaluation. Notably, prior remdesivir-treatment cohort studies indicate that resistant mutations occur at low frequencies, are transient, and are unlikely to contribute significantly to virologic rebound (Tamura et al., 2024).

In conclusion, this study establishes 5-Methyl-3'-dUTP as a potent inhibitor of the SARS-CoV-2 RdRP that functions through a dual mechanism of immediate chain termination and evasion of viral proofreading. Its enhanced incorporation efficiency and irreversible termination further solidify its profile as a promising antiviral candidate. These findings not only provide a strong candidate for further preclinical development against COVID-19 but also open a new avenue for the rational design of next-generation antiviral drugs capable of overcoming viral defense mechanisms.

Author contributions

Acknowledgments

Conflicts of Interest

Data Availability Statement

## 5. Reference


Liu, C., Shi, W., Becker, S. T., Schatz, D. G., Liu, B., & Yang, Y. (2021). Structural basis of mismatch recognition by a SARS-CoV-2 proofreading enzyme. *Science, 373*(6559), 1142-1146. doi:10.1126/science.abi9310

Moeller, N. H., Shi, K., Demir, O., Belica, C., Banerjee, S., Yin, L., . . . Aihara, H. (2022). Structure and dynamics of SARS-CoV-2 proofreading exoribonuclease ExoN. *Proc Natl Acad Sci U S A, 119*(9). doi:10.1073/pnas.2106379119

Tamura, T. J., Choudhary, M. C., Deo, R., Yousuf, F., Gomez, A. N., Edelstein, G. E., . . . Team, P. S. (2024). Emerging SARS-CoV-2 Resistance After Antiviral Treatment. *JAMA Netw Open, 7*(9), e2435431. doi:10.1001/jamanetworkopen.2024.35431